The Strength-Interval Curve for Blood Vessels

Adam J. Connolly[1], Martin J. Bishop[1]

[1] King's College London, London, UK

Abstract

Wavefronts from virtual-electrodes, in response to field-stimulation, are thought to be the main mechanism behind the success of low-energy defibrillation protocols. In this work the concept of the strength-interval curve, usually associated with uni-polar stimulation, is extended to field-stimulation for specific geometrical features - in this case blood-vessels (with realistic fibre architecture and vessel walls) - as the coronary vasculature is known to be an important source of virtual-electrode induced wavefronts. It is shown that, because there is no concept of anodal or cathodal responses in field-stimulation, there is only one strength-interval curve for blood-vessels, and the usual phenomena of make and break excitations are observed for different diastolic intervals. Break excitations occur because regions of de and hyper-polarization are in close proximity due to the resultant virtual-electrode pattern, and they allow excitation at lower field-strengths while the surrounding tissue is relatively refractory. This effect may be important for optimizing low-energy defibrillation protocols.

1.   Introduction

The current strategy for termination of lethal cardiac arrhythmias such as fibrillation, by Implantable Cardioverter Defibrillators (ICDs), is to discharge a high-power capacitor through electrodes implanted in and around the heart. High-energy shocks are thought to activate excitable regions of tissue between the fractionated activation wavefronts, removing the path through which these wavefronts propagate, thus terminating the arrhythmia [1]. However, the high-energies required to defibrillate rapidly deplete the ICD batteries, whilst inappropriate shock therapies cause serious physical pain, damage and psychological stress to the patient and increase mortality rates [2].

Recently, there has been much focus on developing novel strategies for defibrillation that require a fraction of the energy of standard shock treatments [3–6]. It is thought that these techniques are driven by the "Virtual Electrode" (VE) effect, in which heterogeneities (in the form of conductivity discontinuities or varying fibre directions) cause localised regions of depolarisation (and adjacent hyper-polarisation). In contrast to standard high-energy defibrillation where (it can be assumed that) the magnitude of the electric field is sufficiently large such that all heterogeneities emit wavefronts, Low-Energy Defibrillation (LED) relies on the emission of wavefronts only from heterogeneities with sufficiently intense VE depolarizations, which are assumed to be distributed spatially in the myocardium [4].

The relative timing of LED stimulatory pulses, with respect to the dominant arrhythmia cycle length, has been shown [5] to be important in the optimization of LED. In this work, in order to more fundamentally explore the role of VEs from the coronary vasculature in the context of LED, we investigate the effect of field-stimulation on realistic two-dimensional blood-vessel geometries, while the tissue surrounding the vessel is at different levels of refractoriness. In other words, we extend the concept of the strength-interval curve [7, 8] to specific geometrical features (blood-vessels in this case).

2.   Methods

2.1.   Computational models

Two-dimensional blood-vessel geometries, with realistic fibre architecture described by the unit-vector field corresponding to a potential flow (which ensures fibres are tangent to the blood-vessel boundary), were discretized using unstructured triangular finite elements of mean edge length 100 μm. The blood-vessels incorporated a representation of the vessel-lumen wall structure [9, 10], with the relationship between the wall-thickness t and outer radius r given by the empirically derived relationship [11]

$$t = 3.87 r^{0.63}, \qquad (1)$$

corresponding to the human ventricular coronary vasculature. Three different vessel radii were considered: $r_1 = 0.5$, $r_2 = 1.25$ and $r_3 = 3$ mm, which fall within the range of experimentally measured values [11]. A schematic of the computational geometry is shown in Figure 1.
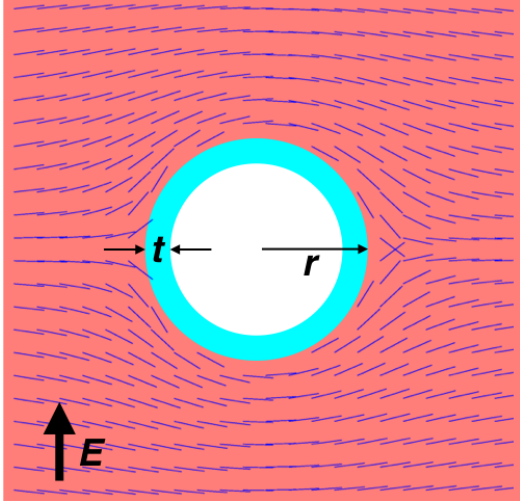
Figure 1. Schematic of the computational domain with a blood-vessel of radius r and a blood-vessel wall of thickness t. The electric field $\boldsymbol{E}$ is aligned with the vertical axis and points upwards. The fibre-field is shown by the blue quiver-plot.

2.2. Computational methods

The finite-element Cardiac Arrhythmia Research Package (CARP) bidomain solver [12] was used to solve the bidomain equations [13] for myocardium. A global stable time-step of 50 ms [14] was used for all simulations. The conductivities of the myocardium ($\boldsymbol{\sigma}_{i,e}$), blood-vessel wall σ_w and blood σ_b inside the vessel were assigned their experimentally measured values (in S/m) of $\boldsymbol{\sigma}_i = (0.17_l, 0.019_t)$ (intracellular) and $\boldsymbol{\sigma}_e = (0.62_l, 0.24_t)$ (extracellular) [15], $\sigma_w = 0.01$ [10] and $\sigma_b = 1.0$ [16] respectively. Ionic dynamics of the myocardium were described by a widely used human ventricular cell model [17] and the myocardium was pre-paced at the single-cell level for 500 beats at a Basic Cycle Length (BCL) of 500 ms, before applying the resultant state variables to all reaction source-terms in the continuum-level bidomain model. The entire myocardium was then excited simultaneously with a single S_1 intracellular stimulus of duration 2 ms (corresponding to the S_1 stimulus in the traditional strength-interval protocol [8]), before applying the S_2 field stimulation (shocks), of 10 ms duration [5, 6] and varying strength at different times during the repolarization of the myocardium. The shock-strength was determined by a bisection algorithm, with a tolerance of 25 mV/cm and an upper bound of 10 V/cm, which tested for successful conduction propagation from the VEs around the blood-vessel.

3. Results

3.1. VE polarization pattern

The VE polarization pattern around the blood-vessels was self-similar, with respect to different vessel radii, due to the imposition of the analytic fibre-field in the myocardium and had a hexapolar morphology [18]; this is shown for the medium-sized vessel in Figure 2. This VE
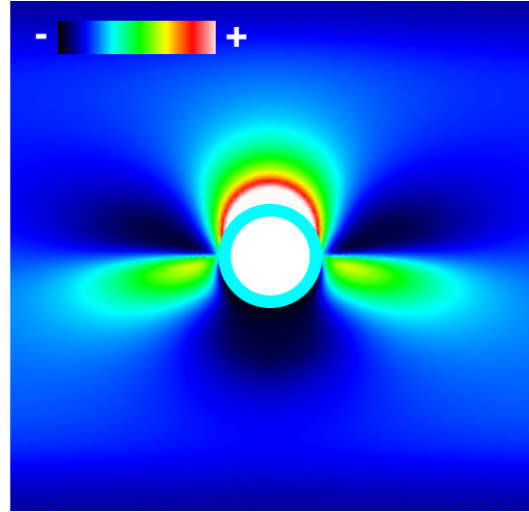

Figure 2. The VE pattern created around a blood-vessel during the shock. Bright colours represent depolarization (+) and dark colours represent hyperpolarization (−).

polarization patten is the opposite of the pattern which would be induced if there was no vessel wall; this is consistent with other works [19] and is due to the low-conductivity vessel wall (σ_w) effectively shielding the flow of extra-cellular current through the vessel cavity [19]. Figure 2 shows that the greatest VE magnitudes were co-incident with the vessel itself and at $\theta = \pi/2, 3\pi/2$, with secondary VEs [20] of lower magnitude located around $\theta = 0, \pi$.

3.2. Strength-interval curves

The strength-interval curves are shown in Figure 3 for the different vessel radii. Visual inspection of the activation wavefronts showed that, for Diastolic Intervals (DI) of less than 310 ms, break-excitation [7, 8] (activation wavefronts which initiate after the cessation of the stimulus pulse and propagate into hyperpolarized regions) occurred, whereas for DIs > 310 ms make-excitation (wavefronts propagate from depolarized regions during the shock) occurred. Make excitations were impossible at DI < 310 ms as the tissue was too refractory for depolarized regions to propagate, however break-excitations were
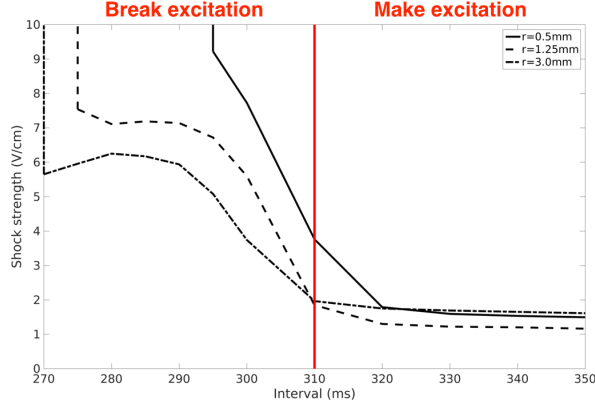
Figure 3. The strength-interval curves for the different blood-vessels. The vertical red line separates the temporal regions of make and break excitation.

possible as regions of hyperpolarization, in close proximity to regions of depolarization, (see Figure 2) were made excitable by the hyperpolarization and wavefronts which propagated into these regions then continued to propagate into the surrounding recovering tissue. A typical break-excitation wavefront propagation pattern in shown in Figure 4 for the middle vessel. For the middle and largest
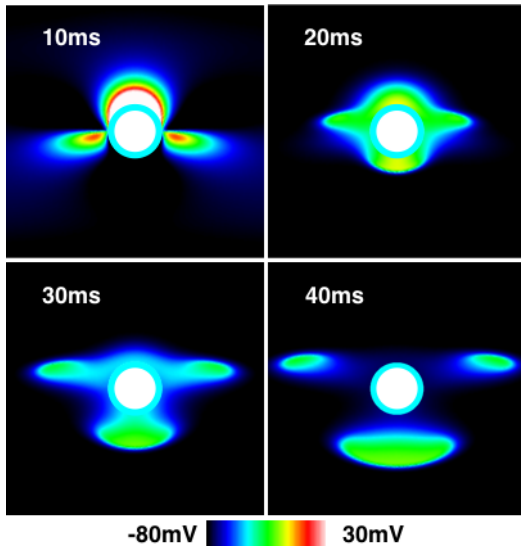

Figure 4. The break-excitation pattern as shown by the transmembrane potential upon cessation of the shock (at 10 ms), for the middle ($r_2 = 1.25$ mm) vessel at DI = 280 ms. The time indicated on the figures refers to the time after the initiation of the shock.

vessels, the strength-interval curves did not monotonically increase with decreasing DI. The shock-strength required for the largest vessel ($r_3 = 3$ mm) increased to a maximum at, DI = 280 ms, before decreasing and the shock-

strength required for the medium vessel ($r_2 = 1.25$ mm) increased to a local maximum at DI = 285 ms before decreasing and then increasing again until DI = 275 ms, when wavefront propagation was not possible at shock-strengths greater than 10 V/cm. In the case of the smallest vessel, the strength-interval curve monotonically increases as DI decreases, however the whole parameter space was not uncovered in this investigation - it is possible that the same trends as the middle and largest vessels would occur for shock strengths greater than 10 V/cm. Note that the APD_{90} for the action potential model used was approximately 290 ms.

4.   Discussion and Conclusions

In this work the strength-interval curves, for realistic blood-vessels of varying radii, in response to field stimulation have been investigated. The strength-interval curves suggest that it is possible to elicit VE-induced wavefront propagation in response to field-stimulation, from break-excitations, at low DIs (while the surrounding tissue is relatively refractory).

Strength-interval curves for blood-vessels, in response to field-stimulation, are not grouped into "anodal" and "cathodal" categories. This is because of the nature of the field-stimulus - swapping the direction of the electric field-vector E simply inverts the VE polarization pattern. Therefore only one strength-interval curve is valid for each blood-vessel geometry.

The strength-interval curves for the sufficiently large vessels (r_2 and r_3) did not monotonically increase (in the parameter-space investigated) for decreasing DI due to the complex VE patterns produced in response to field-stimulation (see Figure 2), and the intrinsic non-linearity of the Hodgkin-Huxley type action potential model used [17]. This observed decrease in the required shock-strength, for earlier DIs, has been reported in other works [7, 8] and is explained (Chapter 4.3 [21]) as thus; for earlier DIs, the depolarization of the surrounding tissue from the S_1 stimulus is higher, meaning that less depolarization from the S_2 (field) stimulus is required to elicit break-excitation. In the temporal region corresponding to break-excitation, the overall shock-strengths required are lower for the larger vessels; this corresponds with the well-known response for circular inclusions to field-stimulation [22]. However, in the temporal region corresponding to make-excitation the largest vessel ($r_3 = 3$ mm) requires the highest shock-strength. This may be because of the non-linear relationship between the wall-thickness and vessel radius (from equation (1)), or due to edge effects (the vessels were surrounded by a square tissue of edge-length 2 cm).

It is known that the coronary vasculature is important in LED [4], and the fact that the strength-interval curve for blood-vessels does not monotonically increase for ear-

lier DIs implies that there is much scope to optimize LED stimulation protocols, in order to minimize the energy required for defibrillation. This is backed up by *in-silico* observations that the timing of LED stimulatory pulses, with respect to the dominant arrhythmia cycle length [5], is important in both the success and energy requirements for LED. It is the authors' opinion that some combination of early and late DI field-stimuli may be optimal in terms of LED energy-efficiency; detailed *in-silico* investigation of LED stimulation protocols will be the focus of our future work.

Acknowledgements

References

[1] Zipes DP, Fischer J, King RM, deB Nicoll A, Jolly WW. Termination of ventricular fibrillation in dogs by depolarizing a critical amount of myocardium. AJC 1975;36(1):37–44.

[2] Larsen GK, Evans J, Lambert WE, Chen Y, Raitt MH. Shocks burden and increased mortality in implantable cardioverter-defibrillator patients. Heart Rhythm 2011; 8:1881–1886.

[3] Fenton FH, Luther S, Cherry EM, Otani NF, Krinsky V, Pumir A, Bodenschatz E, Gilmour RF. Termination of Atrial Fibrillation Using Pulsed Low-Energy Far-Field Stimulation. Circulation 2009;120(6):467–476.

[4] Luther S, Fenton FH, Kornreich BG, Squires A, Bittihn P, Hornung D, Zabel M, Flanders J, Gladuli A, Campoy L, Cherry EM, Luther G, Hasenfuss G, Krinsky VI, Pumir A, Gilmour RF, Bodenschatz E. Low-energy control of electrical turbulence in the heart. Nature 2012;475(7355):235–239.

[5] Rantner LJ, Tice BM, Trayanova NA. Terminating ventricular tachyarrhythmias using far-field low-voltage stimuli: Mechanisms and delivery protocols. Heart Rhythm 2013; 10:1209–17.

[6] Janardhan A, Li W, Fedorov VV, Yeung M, Wallendorf MJ, Schuessler RB, Efimov IR. A novel low-energy electrotherapy that terminates ventricular tachycardia with lower energy than a biphasic shock when antitachycardia pacing fail. JACC 2012;60:2393–2398.

[7] Sidorov VY, Woods MC, Baudenbacher P, Baudenbacher F. Examination of stimulation mechanism and strength-interval curve in cardiac tissue. American Journal of Physiology Heart and Circulatory Physiology 2005; 289(6):H2602–H2615. ISSN 0363-6135.

[8] Kandel MS, Roth BJ. The strength-interval curve in cardiac tissue. Computational and Mathematical Methods in Medicine 2013;1:11.

[9] Gibb M, Bishop M, Burton R, Kohl P, Grau V, Plank G, Rodriguez B. The role of blood vessels in rabbit propagation dynamics and cardiac arrhythmias. Functional Imaging and Modeling of the Heart 2009;5528:268–276.

[10] Bishop MJ, Boyle PM, Plank G, Welsh DG, Vigmond EJ. Modeling the Role of the Coronary Vasculature During External Field Stimulation. IEEE Transactions on Biomedical Engineering 2010;57(10):2335–2345.

[11] Podesser BK, Neumann F, Neumann M, Schreiner W, Wollenek G, Mallinger R. Outer Radius-Wall Thickness Ratio, a Postmortem Quantitative Histology in Human Coronary Arteries. Acta Anatomica Cells Tissues Organs 1998; 163:63–68.

[12] Vigmond E, Hughes M, Plank G, Leon LJ. Computational tools for modeling electrical activity in cardiac tissue. Journal of electrocardiology 2003;36:69–74.

[13] Henriquez CS. Simulating the electrical behavior of cardiac tissue using the bidomain model. Critical reviews in biomedical engineering 1992;21(1):1–77.

[14] Cooper J, Spiteri RJ, Mirams GR. Cellular Cardiac Electrophysiology Modelling with Chaste and CellML. Frontiers in Physiology 2016;511(5):16.

[15] Clerc L. Directional differences of impulse spread in trabecular muscle from mammalian heart. The Journal of Physiology 1976;255(2):335–346.

[16] Visser KR. Electric conductivity of stationary and flowing human blood at low frequencies. In Engineering in Medicine and Biology Society, 1989. Images of the Twenty-First Century, volume 5. 1989; 1540–1542.

[17] ten Tusscher KHWJ. A model for human ventricular tissue. AJP Heart and Circulatory Physiology 2003; 286(4):H1573–H1589.

[18] Hörning M, Takagi S, Yoshikawa K. Wave emission on interacting heterogeneities in cardiac tissue. Phys Rev E 2010;82:021926.

[19] Bishop MJ, Plank G, Vigmond E. Investigating the Role of the Coronary Vasculature in the Mechanisms of Defibrillation. Circulation Arrhythmia and Electrophysiology 2012; 5(1):210–219.

[20] Takagi S, Pumir A, Paza D, Efimov I, Nikolski V, Krinsky V. A physical approach to remove anatomical reentries: a bidomain study. Journal of Theoretical Biology 2004; 230(4):489 – 497. Special Issue in honour of Arthur T. Winfree.

[21] Efimov I, Kroll MW, Tchou PJ. Cardiac Bioelectric Therapy. Springer, 2009.

[22] Pumir A, Krinsky V. Unpinning of a rotating wave in cardiac muscle by an electric field. Journal of Theoretical Biology 1999;199(3):311 – 319. ISSN 0022-5193.

Address for correspondence:

Dr Adam Connolly
King's College London,
St. Thomas' Hospital,
London, SE1 7EH.
adam.connolly@kcl.ac.uk